IEEE Access
Multidisciplinary | Rapid Review | Open Access Journal

Received April 16, 2019, accepted May 31, 2019, date of publication June 10, 2019, date of current version July 1, 2019.

Digital Object Identifier 10.1109/ACCESS.2019.2921802

Photonics-Based High-Resolution 3D Inverse Synthetic Aperture Radar Imaging

XINGWEI YE, (Student Member, IEEE), FANGZHENG ZHANG, (Senior Member, IEEE), YUE YANG, DAIYIN ZHU, AND SHILONG PAN, (Senior Member, IEEE)

Key Laboratory of Radar Imaging and Microwave Photonics, Ministry of Education, Nanjing University of Aeronautics and Astronautics, Nanjing 210016, China

Corresponding authors: Fangzheng Zhang (zhangfangzheng@nuaa.edu.cn) and Shilong Pan (pans@nuaa.edu.cn)

This work was supported in part by the National Natural Science Foundation of China under Grant 61871214, in part by the Natural Science Foundation of Jiangsu Province under Grant BK20180066, in part by the Jiangsu Provincial Program for High-level Talents in Six Areas under Grant DZXX-005, in part by the Jiangsu Provincial 333 Project under Grant BRA2018042, and in part by the Fundamental Research Funds for the Central Universities under Grant NS2018028.

ABSTRACT A photonics-based radar for high-resolution 3D microwave imaging is proposed and demonstrated, in which high range resolution is achieved by employing a wideband linearly frequency modulated signal, and high cross-range resolution in both azimuth and elevation is realized by rotating the target around two orthogonal axes to compose a 2D inverse synthetic aperture. The proposed radar performs photonics-based in-phase/quadrature up-conversion and de-chirp processing in the transmitter and receiver, respectively, which features a compact structure with low-sampling-rate electronics in the receiver. An experiment is carried out. The established radar works in the *K*-band, with bandwidth as large as 8 GHz. Captured echo signals at different rotation angles of the target are processed to a 3D image, in which the voxel values are scattering intensities at different spatial positions.

INDEX TERMS Radar, inverse synthetic aperture radar, microwave photonics, 3D imaging, de-chirp processing.

I. INTRODUCTION

Radar, as its original meaning of RAdio Direction/Detection And Ranging [1], is a system that uses radio signals or microwaves to gather the information of objects in terms of position, velocity, etc. Thanks to the comparatively low propagation loss of microwaves in the atmosphere, radars play an important role in both military and civil applications, especially when the operation in bad weathers is required. In the past few decades, to meet the growing requirements in target recognition, remote sensing and geological survey, plenty of mechanisms have been proposed and studied to improve the resolution of a radar, in which the necessity of wideband waveforms for achieving high range resolution [2], and the requisite large apertures for achieving high cross-range resolution [3] are thoroughly investigated. Recently, with the advantages of low loss, lightweight and flat response over a large bandwidth, microwave photonic techniques have achieved superior performance over pure electronics in the generation [4], [5], frequency-conversion [6], [7], time delay controlling [8], [9], and distribution [10], [11] of wideband microwave signals, which provides promising solutions to implement wideband radar transceivers for high-range-resolution detection [12]. When photonic radar transceivers are utilized along with the methods for enlarging the equivalent baseline or aperture, high-resolution imaging of the targets can be realized [13], [14]. Several inspiring prototypes of such photonics-based radars have been reported for 2D imaging, including the ones with arrayed/distributed antennas [15], [16], multiple-input multiple output (MIMO) principle [17] and relative motion-based synthetic or inverse synthetic aperture [18]–[20].

The successful demonstration of photonics-based high-resolution 2D microwave imaging implies the feasibility of its generalization to 3D imaging, which is gradually a key function of radars to enhance the performance of target location and recognition for security checks, unmanned aerial vehicle detection and pilotless automobiles, etc. One of the approaches to upgrading 2D imaging to 3D imaging is to use two receive antennas to establish an interferometric baseline vertical to the 2D imaging plane [21]. In this case, the phase differences between the two 2D images from the

The associate editor coordinating the review of this manuscript and approving it for publication was Lin Peng.

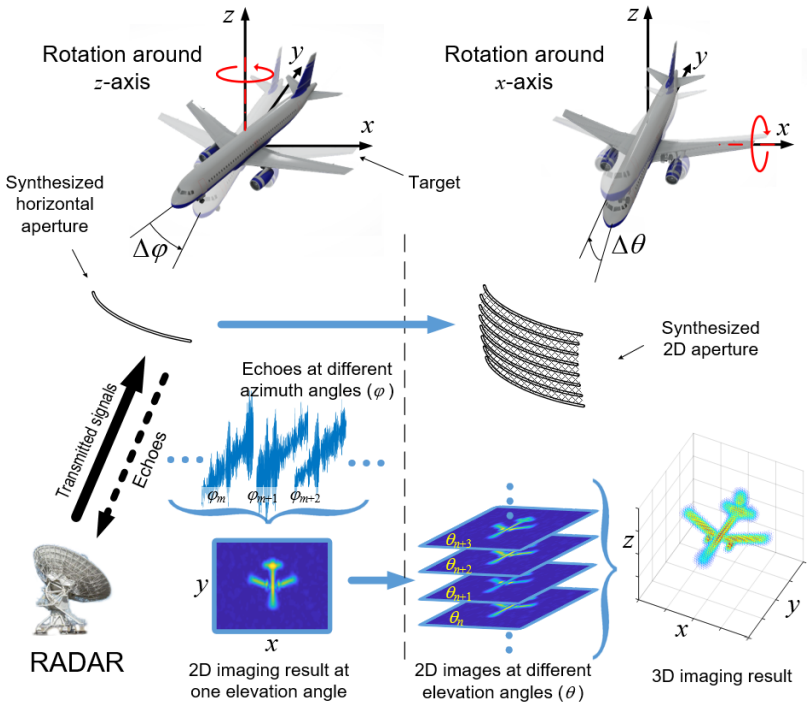

FIGURE 1. Principle of the inverse synthetic aperture radar for 2D imaging and its generalization to 3D imaging.

two antennas are exploited to determine the height of each point. This method is referred to as interferometric inverse synthetic aperture radar (InISAR), when the two 2D images are obtained through inverse synthetic aperture technique. Previously, a photonics-based InISAR has been successfully demonstrated [22], in which 3D image reconstruction of two pairs of cross-placement rotary balls was achieved by fusing 2D images having a resolution as high as 4 cm × 9 cm. To further enhance the performance on the height dimension, the two-element-based interferometric baseline should be extended, in which both the equivalent total length and the number of antennas or sampled points should be effectively increased to improve the resolution and enlarge the ambiguity-free detection region, respectively. In fact, the new vertical baseline or aperture and the existing horizontal aperture for high-cross-range-resolution 2D imaging compose a 2D synthesized aperture which is vertical to the radar-target line of sight (LOS). Basically, such a 2D aperture can be implemented by a planar array of antennas with independent receive channels [23]. The problem associated with this method lies in the high cost since a large 2D aperture for high-resolution imaging could lead to a sharp increase in the number of antennas and receive modules. Many techniques have been proposed to reduce the amount of the receive channels, including the MIMO architecture [24], [25], the scanning by one single antenna or a linear array [26]–[28], and the signal focusing by a parabolic reflector [29]. Demonstrations of 3D imaging radars based on these techniques have shown good results.

In this paper, we propose and demonstrate photonics-based high-resolution 3D inverse synthetic aperture radar (ISAR) imaging, which is implemented by rotating the target to compose a synthesized 2D aperture using only one receive channel. In realizing the 3D imaging, a novel photonic radar transceiver is proposed, in which in-phase/quadrature (I/Q) up-conversion of a baseband linearly frequency modulated (LFM) signal is realized by a dual-polarization dual-parallel Mach–Zehnder modulator (DPol-DPMZM) in the transmitter, and broadband photonics-based de-chirping is implemented in the receiver. A photonics-based radar with a bandwidth of 8 GHz (18-26 GHz) is established and investigated, which verifies the principle of the proposed high-resolution inverse synthetic aperture 3D imaging.

II. PRINCIPLE

Fig. 1 shows the principle of the 3D inverse synthetic aperture radar imaging. Assume that the radar LOS is along the y-axis, so y is the range direction, x (azimuth direction) and z (elevation direction) are the two orthogonal cross-range directions. The inverse synthesis of an aperture on the azimuth direction for 2D imaging is achieved by rotating the target around the z-axis, as shown in the left-hand side of Fig. 1. By recording the echoes at different azimuth angles and combining them coherently with ISAR imaging algorithms, a 2D image can be obtained, of which the range resolution and the azimuth cross-range resolution can be written as [3]

$$\delta y = \frac{c}{2B}, \quad \delta x = \frac{c}{2f_c \Delta\varphi} \tag{1}$$

where c is the propagation speed of the electromagnetic wave, B and f_c are the bandwidth and the center frequency of the transmitted radar signal, respectively, and $\Delta\phi$ is the rotation angle range around the z-axis. The cross-range resolution δx can also be regarded as the Rayleigh resolution of the synthesized aperture on the azimuth direction. Analogous to the x-direction, an inverse synthetic aperture in the elevation direction can also be implemented. To this end, we rotate the target around the x-axis and repeat the 2D imaging at each elevation angle, as shown in the right-hand side of Fig. 1. Then, a 3D ISAR image can be constructed by applying Fourier transform across these complex-valued 2D images [3]. The elevation cross-range resolution of the obtained 3D image is determined by

$$\delta z = \frac{c}{2f_c \Delta\theta} \tag{2}$$

where $\Delta\theta$ is the rotation angle range around the x-axis. In this process, a virtual 2D aperture is scanned and synthesized. Compared to the radar-side 2D aperture implementation in the literature, this 3D imaging method can achieve a higher cross-range resolution with a lower cost, because it is much easier to form a larger viewing angle, which is essential to achieve a higher cross-range resolution, by rotating the target, compared with the method by moving the radar.

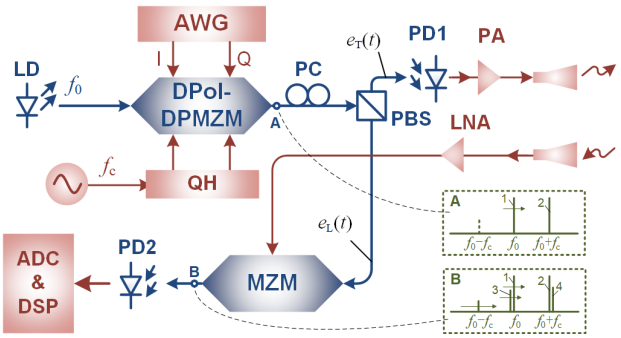

FIGURE 2. Schematic diagram of the proposed photonics-based radar transceiver. LD: laser diode; AWG: arbitrary waveform generator; QH: quadrature hybrid; DPol-DPMZM: dual-polarization dual-parallel Mach-Zehnder modulator; PC: polarization controller; PBS: polarization beam splitter; PD: photodetector; PA: power amplifier; MZM: Mach-Zehnder modulator; LNA: low-noise amplifier; ADC: analog-to-digital conversion; DSP: digital signal processing. (Insets, optical spectra at two key nodes in the transceiver, in which the frequency chirp is illustrated by horizontal arrows).

According to (1), the range resolution along the y direction is determined by the bandwidth of the radar signal. To achieve a high range resolution, we propose a photonics-based radar transceiver to generate and process broadband LFM signals. Fig. 2 shows the schematic diagram of the proposed radar system. In the transmitter, I/Q frequency up-conversion of a complex-valued baseband LFM signal, which has a time duration of T and a frequency range from $-B/2$ to $B/2$, is implemented in the optical domain. To do this, a continuous-wave (CW) optical carrier with a frequency of f_0 from a laser diode is directed to a DPol-DPMZM, which consists of two dual-parallel Mach-Zehnder modulator (DPMZMs) in the X and Y polarizations, respectively. Both of the two DPMZMs are biased at the I/Q modulation mode, i.e., the sub-Mach-Zehnder modulators (MZMs) are biased at the minimum transmission point, and the main MZM is biased at the quadrature point. The optical carrier sent to the DPol-DPMZM is first split equally into two branches, and the signal in each branch is modulated by a DPMZM. The DPMZM in the X polarization is driven by the baseband LFM signal, of which the real and imaginary parts are generated by a two-channel arbitrary waveform generator (AWG). The DPMZM in the Y polarization is driven by two RF signals having the same frequency at f_c but a phase difference of 90°, which is operated at the single sideband-suppressed carrier (SSB-SC) modulation mode. At the output of the DPol-DPMZM, the obtained polarization-multiplexed optical signal contains the following two components in the X and Y polarizations,

$$\begin{bmatrix} e_X(t) \\ e_Y(t) \end{bmatrix} \propto \begin{bmatrix} J_1(\gamma_X)\exp\left(j\left(2\pi f_0 t + \pi k t^2\right)\right) \\ J_1(\gamma_Y)\exp\left(j2\pi\left(f_0 + f_c\right)t\right) \end{bmatrix} \tag{3}$$

where t is defined within $[-T/2, T/2]$, $k = B/T$ is the chirp rate of the baseband LFM signal, $J_n(\cdot)$ is the nth-order Bessel function of the first kind, γ_X and γ_Y are the modulation depths in the corresponding polarization. Under small-signal modulation, the higher order (≥ 2) modulation sidebands can be neglected in obtaining (3). The instantaneous optical spectrum is illustrated in the inset A of Fig. 2, in which the frequency component 1 is a frequency-sweeping tone around f_0 and component 2 is a single tone at (f_0+f_c). After the DPol-DPMZM, a polarization controller (PC) and a polarization beam splitter (PBS) are followed. By adjusting the PC, the polarization state of the modulated lightwave in X or Y polarization is oriented to have an angle of 45° to one of the principal axes of the PBS. The two output signals of the PBS can be expressed as

$$\begin{aligned} e_T(t) &\propto e_X(t) + e_Y(t) \\ e_L(t) &\propto e_X(t) - e_Y(t) \end{aligned} \tag{4}$$

Then, one of the PBS outputs $e_T(t)$ is sent to a photodetector (PD: PD1), of which the photocurrent obtained by frequency beating can be written as

$$i_T(t) \propto \left|e_T(t)\right|^2 \propto \cos\left(2\pi f_c t - \pi k t^2\right) + \mathrm{dc} \tag{5}$$

In (5), an LFM microwave signal centered at f_c is obtained, indicating I/Q up-conversion of the baseband LFM signal is achieved. This signal is filtered and amplified before radiated to the detection area.

In the receiver, the radar echoes collected by the receive antenna are amplified by a low-noise amplifier (LNA) and applied to drive an MZM to modulate the optical reference signal from the other output of the PBS, i.e., $e_L(t)$ in (4). Here, the MZM is biased at the quadrature point. When the radar echo has a time delay of $\Delta\tau$ compared with the

transmitted LFM signal, the output optical signal from the MZM is given by

$$\begin{aligned} e_{\mathrm{B}}(t) &\propto e_{\mathrm{L}}(t)\cdot\left[J_0\left(\gamma_{\mathrm{R}}\right)+2J_1\left(\gamma_{\mathrm{R}}\right)i_{\mathrm{T}}(t-\Delta\tau)\right] \\ &= J_1\left(\gamma_{\mathrm{X}}\right)J_0\left(\gamma_{\mathrm{R}}\right)\exp\left(j\left(2\pi f_0 t+\pi k t^2\right)\right) \\ &\quad -J_1\left(\gamma_{\mathrm{Y}}\right)J_0\left(\gamma_{\mathrm{R}}\right)\exp\left(j2\pi\left(f_0+f_{\mathrm{c}}\right)t\right) \\ &\quad -J_1\left(\gamma_{\mathrm{R}}\right)\left[J_1\left(\gamma_{\mathrm{Y}}\right)P_3-J_1\left(\gamma_{\mathrm{X}}\right)P_4\right] \\ &\quad +J_1\left(\gamma_{\mathrm{R}}\right)\left[J_1\left(\gamma_{\mathrm{X}}\right)P_5-J_1\left(\gamma_{\mathrm{Y}}\right)P_6\right] \end{aligned} \tag{6}$$

where γ_{R} is the modulation depth of the MZM, P_3, P_4, P_5, and P_6 are expressed as

$$\begin{aligned} P_3 &= \exp\left[j\begin{pmatrix}2\pi f_0 t+\pi k t^2+\pi k\Delta\tau^2\\ +2\pi f_{\mathrm{c}}\Delta\tau-2\pi k\Delta\tau t\end{pmatrix}\right] \\ P_4 &= \exp\left[j\begin{pmatrix}2\pi\left(f_0+f_{\mathrm{c}}\right)t-\pi k\Delta\tau^2\\ -2\pi f_{\mathrm{c}}\Delta\tau+2\pi k\Delta\tau t\end{pmatrix}\right] \\ P_5 &= \exp\left[j\begin{pmatrix}2\pi\left(f_0-f_{\mathrm{c}}\right)t+2\pi k t^2+\pi k\Delta\tau^2\\ +2\pi f_{\mathrm{c}}\Delta\tau-2\pi k\Delta\tau t\end{pmatrix}\right] \\ P_6 &= \exp\left[j\begin{pmatrix}2\pi\left(f_0+2f_{\mathrm{c}}\right)t-\pi k t^2-\pi k\Delta\tau^2\\ -2\pi f_{\mathrm{c}}\Delta\tau+2\pi k\Delta\tau t\end{pmatrix}\right] \end{aligned} \tag{7}$$

In this process, small-signal modulation is assumed. In (6) and (7), P_3 and P_4 are the sidebands generated by modulating the optical reference signal with the radar echo, as illustrated by frequency components 3 and 4 in inset B of Fig. 2. After optical-to-electrical conversion in a low-speed PD (PD2), a de-chirped signal is produced as

$$s_{\mathrm{R}}(t)\propto\cos\left[2\pi\left(k\Delta\tau\right)t-2\pi f_{\mathrm{c}}\Delta\tau-\pi k\Delta\tau^2\right] \tag{8}$$

in which the time delay of the radar echo is mapped to the frequency of the obtained signal. According to (8), the distance of the target can be calculated by performing Fourier analysis upon $s_{\mathrm{R}}(t)$. Besides, through the phase variation of the microwave carrier preserved by $2\pi f_{\mathrm{c}}\Delta\tau$ in (8), coherent ISAR imaging can be implemented.

In the proposed radar, the photonics-based I/Q up-conversion of the baseband LFM signal is beneficial to the implementation of both the range and the cross-range resolution. By applying I/Q up-conversion, the sampling rate of the AWG does not need to cover the intermediate frequency carrier which is unavoidable in frequency multiplication-based photonic radar transmitters [30], [31]. Thus, the full bandwidth of the AWG can be used to produce a broadband waveform for higher range resolution. Meanwhile, since the microwave carrier is generated separately from the baseband waveform and is not limited by the bandwidth of the AWG, higher frequency band can be achieved for better cross-range resolution. In addition, the application of photonics-based de-chirp processing can remarkably compress the bandwidths of signals to be digitized, which could effectively release the burden for both analog-to-digital conversion and digital signal processing.

III. EXPERIMENT AND RESULTS

An experiment is carried out to verify the feasibility of the proposed photonics-based 3D ISAR imaging. The radar transceiver is built based on the setup in Fig. 2. In the transmitter, the CW optical carrier from an LD (TeraXion PS-NLL-1550.12) is directed to a DPol-DPMZM (Fujitsu FTM7977) of which the bias voltages are controlled by a modulator bias controller (PlugTech MBC-DPIQ-01). An AWG (Keysight 8195) is used to generate the real part and the imagery part of a positively-chirped baseband LFM signal with a frequency range of –4∼4 GHz, a duty cycle of 66.7%, and a time duration of 10 μs. The microwave carrier at 22 GHz generated by a microwave signal source (Keysight 8257) is split into two branches in a quadrature hybrid for SSB-SC modulation. To boost the optical signal, an erbium-doped fiber amplifier (EDFA) is applied, and an optical band-pass filter (OBPF) is followed to remove the amplified spontaneous emission (ASE) noise. By adjusting a PC, the modulated signals in two polarizations of the DPol-DPMZM are superposed and equally divided by a PBS. One of the PBS output is sent to a PD (Finisar XPDV2120) which yields an 18∼26-GHz LFM signal and completes the I/Q up-conversion. After going through an electrical amplifier and a K-band electrical filter, the up-converted signal is sent to a transmit antenna.

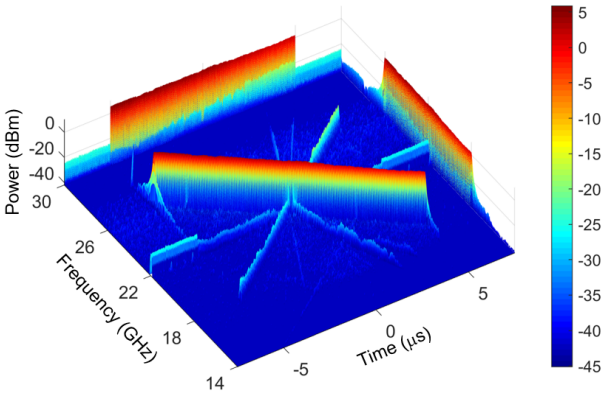

FIGURE 3. Spectrogram of the up-converted signal for radiation. The projection to the time and frequency domains is also performed.

To investigate the performance of the photonics-based I/Q up-conversion, we use a real-time oscilloscope (Keysight 93304) to capture the transmit signal and conduct the signal analysis in the digital domain. The spectrogram obtained from the short-time Fourier transform, and the profiles in the time and the frequency domain are shown in Fig. 3. As can be seen, a negatively-chirped signal covering a broad bandwidth of 8 GHz and centered at 22 GHz is successfully generated in a 10-μs time window. In Fig. 3, some spurs exist, of which the major ones are the complementarily-chirped signal within the time window and the 22-GHz single-tone signal out of the time window. These spurs mainly come from the residual modulation sidebands due to the unideal bias of the DPol-DPMZM. Since the spurs are at least 20 dB lower than the desired signal and their chirp rates are different from the required signal, the negative influences of the spurs can be omitted in the system.

The other output signal from the PBS is used as the optical carrier in the receiver. It is sent to an MZM (Fujitsu FTM7938) driven by the radar echoes that are collected by a receive antenna and amplified by an LNA. Downstream of the MZM, a PD (Conquer Co.) converts the optical signal into the electrical domain and gives the de-chirped results which then pass through a low-pass filter to reject unwanted components at higher frequencies. The filtered signals are digitized and recorded by the real-time oscilloscope before processed in the digital domain.

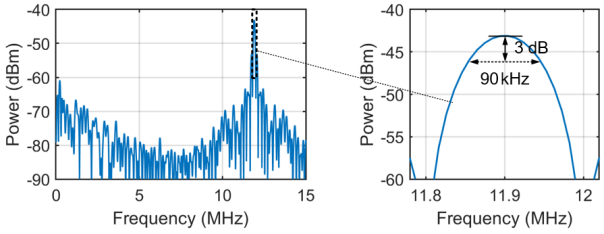

FIGURE 4. Spectrum of a de-chirped signal and the zoom-in view of the spectral peak.

The range resolution that can be achieved by the proposed radar transceiver is evaluated by the spectral peak width of the de-chirped signal. For simplicity, we direct the signal for radiation immediately to the driving port of the MZM in the receiver to imitate the detection of a single point target. The spectrum of the de-chirped signal is plotted in Fig. 4. From the zoom-in view of the spectral peak at 11.9 MHz, it is found that the 3-dB peak width is 90 kHz. The corresponding range resolution is calculated to be 1.904 cm which is quite close to the theoretical resolution (1.875 cm) determined by the signal bandwidth [3].

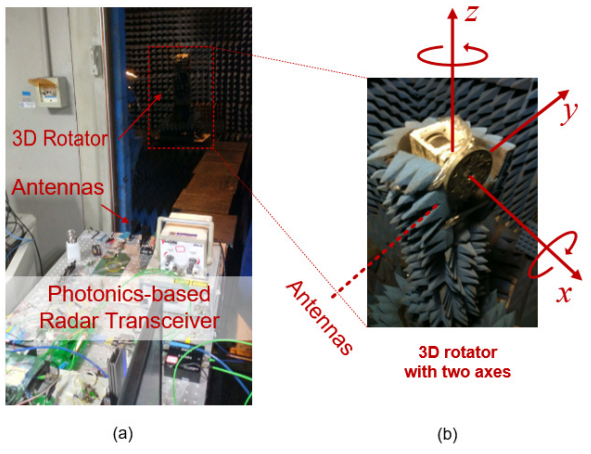

FIGURE 5. Photographs of (a) the experimental setup and (b) the rotator used in the experiment.

Based on the proposed photonic radar transceiver, a 3D imaging system is established as shown in Fig. 5(a), in which two K-band horn antennas are oriented to a 3D rotator in 4-meter distance. As shown in Fig. 5(b), the 3D rotator placed in an anechoic chamber has a vertical axis and a rotatable plate to perform the rotation of targets in azimuth direction and elevation direction, respectively. The targets under radiation are mounted onto the rotatable plate through three plastic sticks. Figure 5(b) illustrates the coordinate system used for the 3D imaging. Here, the radar LOS is along the y-axis. The azimuth rotation is around the z-axis, and the elevation rotation is around the x-axis. The rotation center of the 3D rotator is at the origin of the coordinate system. In the experiment, the azimuth rotation is repeated on different elevation angles. The effective scanned angular regions on azimuth direction and elevation directions are 34° and 30°, respectively. The total scanning time is about ten minutes in our experiment, which is determined by the rotating speed of the rotator.

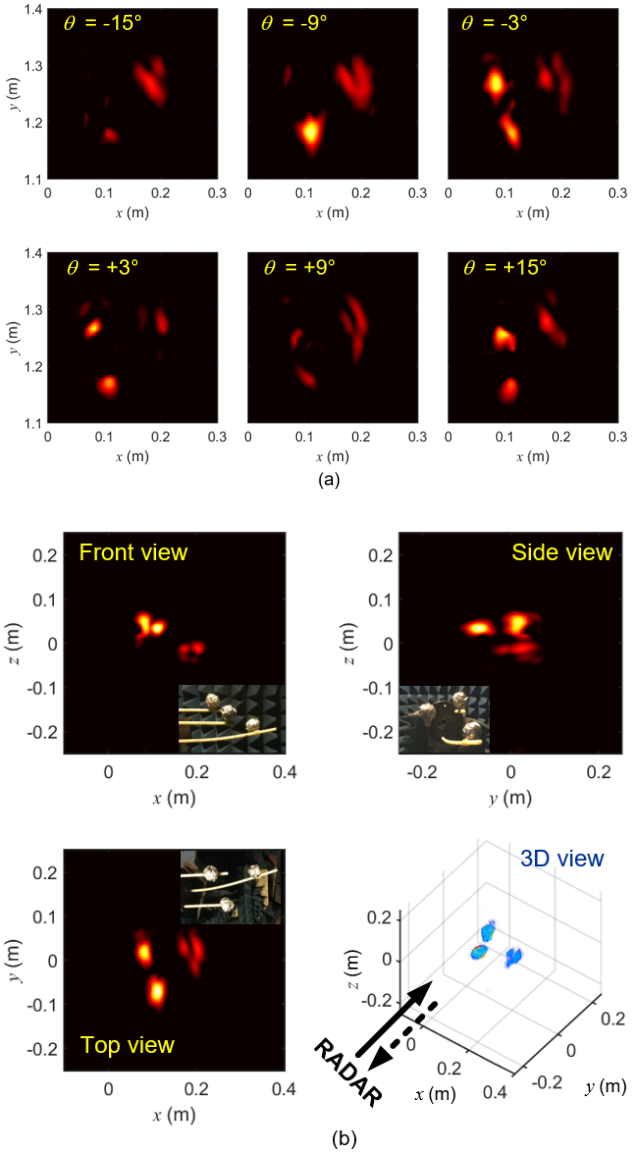

FIGURE 6. Imaging results of three reflective balls. (a) 2D images at different elevation angles. (b) 3D results illustrated by a 3D view and 2D views from maximum value projection onto coordinate planes. The placement of the three balls is shown as the photographs.

First of all, three reflective balls are used as a simple set of targets. Their positions are shown in the photographs in Fig. 6.

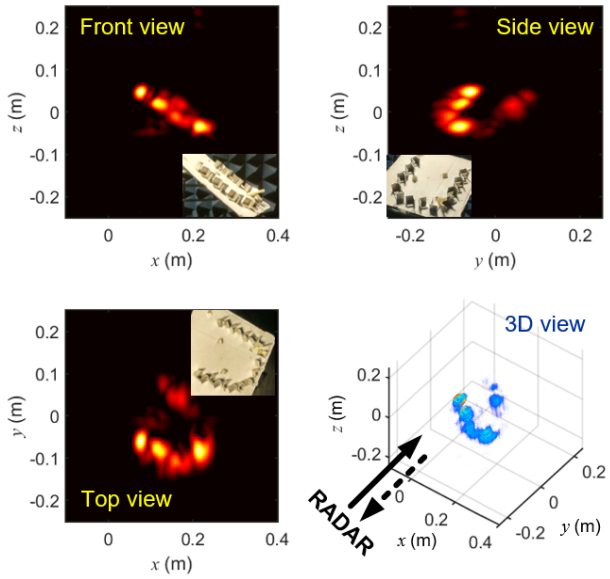

FIGURE 7. Results of 3D imaging of a set of U-shape-arranged corner reflectors. Photographs of the targets from different 2D views are also shown for comparison.

During the scanning along elevation direction, 2D images obtained from azimuth rotations on different elevation angles are plotted in Fig. 6(a), in which the contribution of background is subtracted from the original results. In Fig. 6(a), the difference between any two 2D images is obvious. This is due to the fact that the interference between echoes varies with different elevation angles. In addition, part of the targets may blur or even disappear in the 2D images, implying the limitation of 2D imaging in target recognition. By coherently combining the multiple 2D images, a 3D image is achieved, as shown in Fig. 6(b). In Fig. 6(a), the 3D image of the targets is presented in both 2D and 3D views, in which the 2D views are formed by maximum value projection [27] to coordinate planes, and the 3D view is the scatterplot of the points whose intensity values are larger than 5% of the peak one in the region. We can see that the imaging result coincides with the locations of the three balls, which confirms the feasibility of the proposed 3D imaging radar.

Finally, a set of U-shape-arranged corner reflectors that are stuck on a cardboard are used as the targets. The 2D and 3D views of the 3D imaging results are shown in Fig. 7. Comparing the imaging results with the actual scene shown in the inset of each picture, it is found that the geometry characteristics reconstructed by the 3D imaging match well with the features of the targets. However, since the transmitted radar signal could be blocked by the targets nearer to the radar, parts of the corner reflectors are missing in the 3D image. To overcome the problem of overshadowing, a broadened angular region for scanning can be applied along with the ISAR algorithms considering rotational motion compensation [32].

IV. CONCLUSION

In conclusion, we have proposed and demonstrated a 2D rotation-based 3D inverse synthetic aperture imaging radar applying a broadband photonics-based radar transceiver. An experiment was conducted over the frequency of 18∼26 GHz, in which 3D imaging of different targets were performed with good imaging results. The proposed 3D imaging radar can effectively enhance the target recognition and it may play an important role in applications such as security checks.

REFERENCES

[1] M. Skolnik, "An introduction and overview of radar," in *Radar Handbook*, 3rd ed. New York, NY, USA: McGraw-Hill, 2008, pp. 1.1–1.24.
[2] M. A. Richards, "Pulsed radar data acquisition," in *Fundamentals of Radar Signal Processing*, 2nd ed. New York, NY, USA: McGraw-Hill, 2014, pp. 183–229.
[3] C. Özdemiir, "Inverse synthetic aperture radar imaging and its basic concepts," in *Inverse Synthetic Aperture Radar Imaging With MATLAB Algorithms*. Hoboken, NJ, USA: Wiley, 2012, pp. 121–186.
[4] Y. Gao, A. Wen, W. Jiang, D. Liang, W. Liu, and S. Xiang, "Photonic microwave generation with frequency octupling based on a DP-QPSK modulator," *IEEE Photon. Technol. Lett.*, vol. 27, no. 21, pp. 2260–2263, Nov. 1, 2015.
[5] P. Zhou, F. Zhang, X. Ye, Q. Guo, and S. Pan, "Flexible frequency-hopping microwave generation by dynamic control of optically injected semiconductor laser," *IEEE Photon. J.*, vol. 8, no. 6, Dec. 2016, Art. no. 5501909.
[6] Z. Tang and S. Pan, "Image-reject mixer with large suppression of mixing spurs based on a photonic microwave phase shifter," *J. Lightw. Technol.*, vol. 34, no. 20, pp. 4729–4735, Oct. 15, 2016.
[7] J. Li, J. Xiao, X. Song, Y. Zheng, C. Yin, Q. Lv, Y. Fan, F. Yin, Y. Dai, and K. Xu, "Full-band direct-conversion receiver with enhanced port isolation and I/Q phase balance using microwave photonic I/Q mixer," *Chin. Opt. Lett.*, vol. 15, no. 1, 2017, Art. no. 010014.
[8] R. Rotman, M. Tur, and L. Yaron, "True time delay in phased arrays," *Proc. IEEE*, vol. 104, no. 3, pp. 504–518, Mar. 2016.
[9] X. Ye, D. Zhu, Y. Zhang, S. Li, and S. Pan, "Analysis of photonics-based RF beamforming with large instantaneous bandwidth," *J. Lightw. Technol.*, vol. 35, no. 23, pp. 5010–5019, Dec. 1, 2017.
[10] K. Y. Lau, G. F. Lutes, and R. L. Tjoelker, "Ultra-stable RF-over-fiber transport in NASA antennas, phased arrays and radars," *J. Lightw. Technol.*, vol. 32, no. 20, pp. 3440–3451, Oct. 15, 2014.
[11] J. Wei, F. Zhang, Y. Zhou, D. Ben, and S. Pan , "Stable fiber delivery of radio-frequency signal based on passive phase correction," *Opt. Lett.*, vol. 39, no. 11, pp. 3360–3362, Jun. 2014.
[12] S. L. Pan and J. Yao, "Photonics-based broadband microwave measurement," *J. Lightw. Technol.*, vol. 35, no. 16, pp. 3498–3513, Aug. 15, 2017.
[13] P. Ghelfi, F. Laghezza, F. Scotti, G. Serafino, A. Capria, S. Pinna, D. Onori, C. Porzi, M. Scaffardi, A. Malacarne, V. Vercesi, E. Lazzeri, F. Berizzi, and A. Bogoni, "A fully photonics-based coherent radar system," *Nature*, vol. 507, no. 7492, pp. 341–345, Mar. 2014.
[14] G. Serafino, F. Amato, S. Maresca, L. Lembo, P. Ghelfi, and A. Bogoni, "Photonic approach for on-board and ground radars in automotive applications," *IET Radar, Sonar Navigat.*, vol. 12, no. 10, pp. 1179–1186, Oct. 2018.
[15] Z. G. Tegegne, C. Decroze, P. D. Bin, T. Fromenteze, and C. Aupetit-Berthelemot, "Single channel microwave photonics digital beamforming radar imaging system," *J. Lightw. Technol.*, vol. 36, no. 3, pp. 675–681, Feb. 1, 2018.
[16] X. Xiao, S. Li, S. Peng, D. Wu, X. Xue, X. Zheng, and B. Zhou, "Photonics-based wideband distributed coherent aperture radar system," *Opt. Express*, vol. 26, no. 26, pp. 33783–33796, 2018.
[17] F. Zhang, B. Gao, and S. Pan, "Photonics-based MIMO radar with high-resolution and fast detection capability," *Opt. Express*, vol. 26, no. 13, pp. 17529–17540, 2018.
[18] R. Li, W. Li, M. Ding, Z. Wen, Y. Li, L. Zhou, S. Yu, T. Xing, B. Gao, Y. Luan, Y. Zhu, P. Guo, Y. Tian, and X. Liang, "Demonstration of a microwave photonic synthetic aperture radar based on photonic-assisted signal generation and stretch processing," *Opt. Express*, vol. 25, no. 13, pp. 14334–14340, 2017.
[19] A. Wang, J. Wo, X. Luo, Y. Wang, W. Cong, P. Du, J. Zhang, B. Zhao, J. Zhang, Y. Zhu, J. Lan, and L. Yu, "Ka-band microwave photonic ultra-wideband imaging radar for capturing quantitative target information," *Opt. Express*, vol. 26, no. 16, pp. 20708–20717, 2018.

[20] Y. Yao, F. Zhang, Y. Zhang, X. Ye, D. Zhu, and S. Pan, "Demonstration of ultra-high-resolution photonics-based kaband inverse synthetic aperture radar imaging," in *Proc. Opt. Fiber Commun. Conf. Expo.*, San Diego, CA, USA, Mar. 2018, pp. 1–3, Paper Th3G. 5.
[21] M. Martorella, D. Stagliano, F. Salvetti, and N. Battisti, "3D interferometric ISAR imaging of noncooperative targets," *IEEE Trans. Aerosp. Electron. Syst.*, vol. 50, no. 4, pp. 3102–3114, Oct. 2014.
[22] D. Wu, S. Li, X. Xue, X. Xiao, S. Peng, and X. Zheng, "Photonics based microwave dynamic 3D reconstruction of moving targets," *Opt. Express*, vol. 26, no. 21, pp. 27659–27667, 2018.
[23] S. S. Ahmed, A. Schiessl, F. Gumbmann, M. Tiebout, S. Methfessel, and L. Schmidt, "Advanced microwave imaging," *IEEE Microw. Mag.*, vol. 13, no. 6, pp. 26–43, Sep. 2012.
[24] D. Bleh, M. Rösch, M. Kuri, A. Dyck, A. Tessmann, A. Leuther, S. Wagner, B. Weismann-Thaden, H.-P. Stulz, M. Zink, M. Rießle, R. Sommer, J. Wilcke, M. Schlechtweg, B. Yang, and O. Ambacher, "W -band time-domain multiplexing FMCW MIMO radar for far-field 3-D imaging," *IEEE Trans. Microw. Theory Techn.*, vol. 65, no. 9, pp. 3474–3484, Sep. 2017.
[25] X. Xu and Y. Liu, "Three-dimensional interferometric MIMO radar imaging for target scattering diagnosis," *J. Radars*, vol. 7, no. 6, pp. 655–663, Dec. 2018.
[26] D. M. Sheen, D. L. McMakin, and T. E. Hall, "Three-dimensional millimeter-wave imaging for concealed weapon detection," *IEEE Trans. Microw. Theory Techn.*, vol. 49, no. 9, pp. 1581–1592, Sep. 2001.
[27] D. Sheen, D. McMakin, and T. Hall, "Near-field three-dimensional radar imaging techniques and applications," *Appl. Opt.*, vol. 49, no. 19, pp. E83–E93, 2010.
[28] T.-F. Tseng, J.-M. Wun, W. Chen, S.-W. Peng, J.-W. Shi, and C.-K. Sun, "High-depth-resolution 3-dimensional radar-imaging system based on a few-cycle W-band photonic millimeter-wave pulse generator," *Opt. Express*, vol. 21, no. 12, pp. 14109–14119, 2013.
[29] G. Charvat, A. Temme, M. Feigin, and R. Raskar, "Time-of-flight microwave camera," *Sci. Rep.*, vol. 5, Oct. 2015, Art. no. 14709.
[30] F. Zhang, Q. Guo, Y. Zhang, Y. Yao, P. Zhou, D. Zhu, and S. Pan, "Photonics-based real-time and high-resolution ISAR imaging of noncooperative target," *Chin. Opt. Lett.*, vol. 15, no. 11, 2017, Art. no. 112801.
[31] X. Ye, F. Zhang, Y. Yang, and S. Pan, "Photonics-based radar with balanced I/Q de-chirping for interference-suppressed high-resolution detection and imaging," *Photon. Res.*, vol. 7, no. 3, pp. 265–272, 2019.
[32] V. C. Chen and M. Martorella, "ISAR Motion Compensation," in *Inverse Synthetic Aperture Radar Imaging: Principles, Algorithms and Applications*. Edison, NJ, USA: SciTech, 2014, pp. 77–103.

XINGWEI YE (S'14) received the B.S. degree from the Nanjing University of Aeronautics and Astronautics, Nanjing, China, in 2014, where he is currently pursuing the Ph.D. degree with the Key Laboratory of Radar Imaging and Microwave Photonics, Ministry of Education.

His main research interests include photonic technologies for RF beamforming, synthetic aperture imaging, and direct sampling.

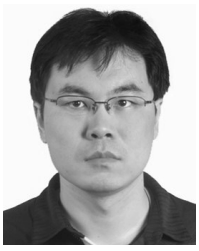

FANGZHENG ZHANG (S'10–M'13–SM'19) received the B.S. degree from the Huazhong University of Science and Technology, Wuhan, China, in 2008, and the Ph.D. degree from the Beijing University of Posts and Telecommunications, Beijing, China, in 2013.

He is currently a Full Professor with the College of Electronic and Information Engineering, Nanjing University of Aeronautics and Astronautics. His current research interests include microwave photonics and all-optical signal processing.

YUE YANG received the B.S. degree from the Nanjing University of Aeronautics and Astronautics, Nanjing, China, in 2018, where he is currently pursuing the Ph.D. degree with the Key Laboratory of Radar Imaging and Microwave Photonics, Ministry of Education.

His main research interest includes photonics-based radars for high-resolution imaging.

DAIYIN ZHU was born in Wuxi, China, in 1974. He received the B.S. degree in electronic engineering from Southeast University, Nanjing, China, in 1996, and the M.S. and Ph.D. degrees in electronics from the Nanjing University of Aeronautics and Astronautics (NUAA), Nanjing, China, in 1998 and 2002, respectively. From 1998 to 1999, he was a Guest Scientist with the Institute of Radio Frequency Technology, German Aerospace Center, where he was involved in the field of SAR interferometry. In 1998, he joined the Department of Electronic Engineering, NUAA, where he is currently a Professor. He has developed algorithms for several operational airborne SAR systems. His current research interests include radar imaging algorithms, SAR/ISAR autofocus techniques, SAR ground moving target indication, and SAR interferometry. In 2002, he received the Award of Defense Science and Technology, concerning airborne SAR system design and signal processing.

SHILONG PAN (S'06–M'09–SM'13) received the B.S. and Ph.D. degrees in electronic engineering from Tsinghua University, Beijing, China, in 2004 and 2008, respectively.

From 2008 to 2010, he was a Vision 2010 Postdoctoral Research Fellow of the Microwave Photonics Research Laboratory, University of Ottawa, Canada. He has authored or coauthored over 420 research papers, including more than 230 papers in peer-reviewed journals and 190 papers in conference proceedings. He joined the College of Electronic and Information Engineering, Nanjing University of Aeronautics and Astronautics, China, in 2010, where he is currently a Full Professor and an Executive Director of the Key Laboratory of Radar Imaging and Microwave Photonics, Ministry of Education. His research has focused on microwave photonics, which includes optical generation and processing of microwave signals, analog photonic links, photonic microwave measurements, and integrated microwave photonics.

Prof. Pan is a Fellow of the SPIE and the IET and a Senior Member of the OSA. He was selected to receive the IEEE Photonics Society Distinguished Lecturer Award, the OSA Outstanding Reviewer Award, in 2015, a Top Reviewer of the IEEE/OSA Journal of Lightwave Technology, in 2016 and 2018, and the Publons Peer Reviewer Award, in 2018. He received the Scientific and Technological Innovation Leading Talents Award from the National Ten Thousand Plan, in 2018. He is a Steering Committee Member of the IEEE International Topical Meeting on Microwave Photonics and the International Conference on Optical Communications and Networks. He has also served as a Chair of a number of international conferences, symposia, and workshops, including the TPC Chair of the International Conference on Optical Communications and Networks, in 2015, and the TPC Co-Chair of the IEEE International Topical Meeting on Microwave Photonics, in 2017. He is currently an Associate Editor of *Electronics Letters*, a Topical Editor of *Chinese Optics Letters*, and a Technical Committee Member of the IEEE MTT-3 Microwave Photonics.